Reconnection and scale-free avalanching in a driven current-sheet model

Alex J. Klimas,[1] Vadim M. Uritsky,[2] Dimitris Vassiliadis,[3] and Daniel N. Baker[4]

Received 12 May 2003; revised 18 August 2003; accepted 2 September 2003; published 27 February 2004.

[1] *Uritsky et al.* [2002], through a study of Polar UVI auroral image sequences, have produced a set of scale-free probability distributions for several characteristic properties of the evolving bright emission regions in the nightside auroral oval. These distributions almost certainly reflect the dynamics of the plasma sheet. A scale-free avalanching process involving reconnection and/or current diversion over an exceptionally broad range of spatiotemporal scales is implied. The most straightforward, and at present sole, explanation for this behavior is that the plasma sheet dynamics is in the neighborhood of self-organized criticality (SOC). However, the auroral images provide only an indirect measure of the plasma sheet dynamics. Confirmation of this state in the plasma sheet would require multispatiotemporal-scale in situ plasma sheet studies that, with the advent of multispacecraft missions, are now possible. To suggest specific tests for such studies, a numerical current-sheet model has been constructed and analyzed to develop the properties and requirements of SOC in a plasma physical setting. The model incorporates the anomalous resistivity of a current-driven kinetic instability into a two-dimensional resistive MHD system. The disparate scales of these two systems enable multiscale behavior in the intervening range. Several novel features in the model's behavior are enabled through the assumption of hysteresis in the kinetic instability threshold. Under steady loading of plasma containing a reversed magnetic field topology, an irregular loading-unloading cycle is established in which unloading is due primarily to annihilation at the field reversal. Following a loading interval during which the current-sheet supporting the field reversal thins and intensifies, an unloading event originates at a localized reconnection site that then becomes the source of waves of unstable current sheets. These current sheets propagate away from the reconnection site, each leaving a trail of anomalous resistivity behind. An expanding cascade of field line merging results. Some statistical properties of this cascade are examined. It is shown that the diffusive contribution to the Poynting flux in these cascades occurs in bursts, whose duration, integrated size, and total energy content exhibit scale-free power law probability distributions over large ranges of scales. Although not conclusive, these distributions do provide strong evidence that the model has evolved into SOC. *INDEX TERMS:* 2764 Magnetospheric Physics: Plasma sheet; 2753 Magnetospheric Physics: Numerical modeling; 3220 Mathematical Geophysics: Nonlinear dynamics; 7835 Space Plasma Physics: Magnetic reconnection; 7843 Space Plasma Physics: Numerical simulation studies; *KEYWORDS:* self-organized criticality, plasma sheet, simulation, scale-free, avalanche distributions, loading-unloading cycle

Citation: Klimas, A. J., V. M. Uritsky, D. Vassiliadis, and D. N. Baker (2004), Reconnection and scale-free avalanching in a driven current-sheet model, *J. Geophys. Res.*, *109*, A02218, doi:10.1029/2003JA010036.

1. Introduction

[2] The magnetospheric substorm is a complicated, multifaceted phenomenon. At its core, however, there is one fundamental process, the loading and unloading of magnetic flux and energy [*Baker et al.*, 1999]. A southward turning of the interplanetary magnetic field leads to loading in the magnetotail. Unloading takes place when a global plasma sheet instability releases the stresses that this loading produces. This process may be shortened by external disturbances in the solar wind (external triggering) [*Lyons et*

[1]Laboratory for Extraterrestrial Physics, NASA Goddard Space Flight Center, Greenbelt, Maryland, USA.
[2]Institute of Physics and Physics Department, St. Petersburg State University, St. Petersburg, Russia.
[3]Universities Space Research Association, NASA Goddard Space Flight Center, Greenbelt, Maryland, USA.
[4]Laboratory for Atmospheric and Space Physics, University of Colorado, Boulder, Colorado, USA.

0148-0227/04/2003JA010036

al., 1997; *Blanchard et al.*, 2000; *Lyons*, 2000; *Russel*, 2000], or it may proceed to completion (internal triggering). In either case, the plasma sheet dynamics controls the transition to global instability at the substorm onset time. Clearly, then, understanding the plasma sheet dynamics is central to understanding the substorm cycle.

[3] It is known that in a largely quiescent background the plasma sheet contains fast flow bursts that are grouped together into 10–20 min events called bursty bulk flows (BBFs) [*Baumjohann et al.*, 1990; *Angelopoulos et al.*, 1992, 1994, 1996, 1999a; *Zesta et al.*, 2000; *Nakamura et al.*, 2001a, 2001b]. These BBFs are thought to be generated by reconnection in the plasma sheet that is localized to spatial scales of no more than 1–2 R_E; plasmoid releases have been shown to be associated with these fast flows [*Ieda et al.*, 2001]. BBFs have been observed over a large portion of the plasma sheet and, although correlated with substorm activity, they can be detected at any time in the substorm cycle. The fast flows in the plasma sheet act like jets in a fluid, producing strong eddy turbulence. Long-time statistical analysis yields an eddy scale size $\simeq$1.6 R_E and an eddy turnover time $\simeq$2.3 min while fluctuations in the magnetic field are found comparable in magnitude to its mean value [*Borovsky et al.*, 1997]. However, it also has been shown that the turbulence is intermittent at large spatial scales ($\simeq$5 R_E) [*Angelopoulos et al.*, 1999b] and at very small scales, perhaps as small as ion kinetic scales [*Vörös et al.*, 2003]. Substorm onset studies that do not consider these known plasma sheet properties cannot be considered reliable.

[4] It has been shown that on large spatiotemporal scales the magnetosphere behaves as a low-dimensional dynamical system [*Sharma*, 1995; *Vassiliadis et al.*, 1995; *Klimas et al.*, 1996]. The global substorm cycle is a manifestation of this dynamic. The role of the plasma sheet in the substorm cycle must be understood in terms of the interaction of its broadband, multiscale, high-dimensional turbulence with the low-dimensional global magnetosphere.

[5] *Chang* [1992a, 1992b, 1998, 1999] and *Chang and Wu* [2002] have shown that a system that is in the state known as self-organized criticality (SOC) [*Bak et al.*, 1987, 1988; *Bak*, 1997; *Jensen*, 1998] can exhibit apparent low-dimensional global dynamics that is, nevertheless, structured about a high-dimensional internal avalanching process. Evidence in support of SOC has accumulated since Chang's suggestion that the dynamics of the magnetotail can be understood within this framework. *Uritsky et al.* [2002], using an extension of a method introduced by *Lui et al.* [2000], have produced the most convincing of this evidence through a detailed study of two long sequences of Polar UVI images. A threshold in the image intensity was applied and then the spatiotemporal evolution of bright regions in the nightside aurora that reached above this threshold was studied. These bright regions were treated exactly as though they were avalanches in a numerical running-sandpile experiment [*Becker et al.*, 1995] and were thus shown to exhibit the characteristic behavior of systems in SOC. No other explanation for these results is available at present. However, the location of this presumed SOC dynamics and the physical mechanism responsible for it is open to speculation.

[6] Systems in SOC are spatially extended and subject to loading and unloading of a quantity that is otherwise conserved. The transport of the conserved quantity through the system is controlled by a local threshold instability; when the instability is excited the conserved quantity moves toward the region or boundary where unloading takes place. Under certain conditions, the system may be driven to the neighborhood of a critical point in its dynamics; the system self-organizes toward criticality in response to being loaded. One characteristic of this neighborhood is that the local threshold instability resides near its excitation threshold throughout the spatially extended system. There are three important consequences of this characteristic: (1) the requirement of marginal stability throughout the system may result in relatively simple global dynamics; (2) the excitation of the local instability at one position may lead to a cascade of local instabilities, conventionally called an avalanche, and distributions of avalanche properties may exhibit no characteristic scales; (3) avalanches of any size, including system-wide avalanches, may result from small external perturbations (external triggering) since the entire system is sensitive to any perturbation.

[7] The system described in the preceding paragraph suggests the magnetotail as the location for the SOC dynamics. The conserved quantity would be magnetic flux or energy, which is transported through the system by the action of a local instability that leads to localized reconnection. This suggestion is strengthened by the well-known relationship of plasma sheet fast flows and localized reconnection to auroral brightening. This relationship has been demonstrated for localized reconnection events isolated in the midst of otherwise quiet intervals as well as for substorm events. *Ieda et al.* [2001] have found 24 fast flow events in their study of GEOTAIL plasma sheet data for which simultaneous Polar UVI images were available. In every case, auroral brightening was found associated with the in situ fast flow. If the inverse relationship holds to a significant degree, then the indications of SOC dynamics obtained by *Uritsky et al.* [2002] through their UVI auroral image study could be interpreted as a reflection of the dynamics of the plasma sheet. From this perspective, the plasma sheet is a scale-free avalanching system whose dynamics is controlled by a local instability associated with localized reconnection. Rather than a single global instability, substorm onset must be viewed as a cascade of these local instabilities in strongly turbulent plasma whose characteristic time and length scales are quite small when compared to the system size [*Chang and Wu*, 2002; *Chang et al.*, 2002].

[8] While the one-to-one relationship between plasma sheet fast flows and auroral brightening is well established, the inverse relationship is not so definite. To proceed further toward understanding the dynamics of the plasma sheet, it is clearly necessary to focus on the plasma sheet itself. The multispacecraft Cluster II and Magnetospheric Multiscale (MMS) missions could be particularly well suited for searching the plasma sheet for possible multiscale spatiotemporal dynamics. However, it is not clear at this time exactly what to look for. Much of what is known about SOC has been learned through studies of various types of sandpile models, and such models have been used to describe the magnetotail dynamics [*Chapman et al.*, 1998,

1999; *Watkins et al.*, 1999; *Chapman*, 2000]. To understand the specific details of the plasma sheet behavior that would be involved if it were indeed in SOC, it is necessary to go beyond such models.

[9] *Lu* [1995] has studied a continuum model that exhibits some of the behavior of discrete sandpile models when they are in SOC. *Klimas et al.* [2000] noted that a variant of the Lu model could be obtained through a reduction to one dimension of a resistive MHD current-sheet model in which the resistance is anomalous and created through the excitation of a current-driven instability This one-dimensional (1-D) current-sheet model has been shown. [*Uritsky et al.*, 2001a, 2001b] to evolve naturally into SOC, as it is understood today through the mean-field theory of *Vespignani and Zapperi* [1998]. Klimas et al. also noted that the reduction to one dimension could be reversed to produce, starting with the one-dimensional model, a sequence of ever more realistic plasma physical models of SOC in the magnetotail. In this paper, we present the first results from our study of the next model in this sequence, a two-dimensional driven current-sheet model. The model is introduced below in section 2 and the manner in which it is integrated to induce it into a stationary state involving a loading-unloading cycle is discussed in section 3. The onset of one of these unloading events in the model is discussed in detail in section 4. It is shown that the unloading event originates at a localized reconnection site, which then becomes the locus of an expanding cascade of field line merging. This cascade suggests a possible avalanching mechanism for the plasma sheet. A discussion of some statistical properties of the cascade follows.

[10] Scale-free distributions (power laws with no peaks or valleys) of various avalanche properties are characteristic of systems in SOC. Alone, such distributions do not constitute a proof that the system is in SOC but, depending on other relevant factors, they may constitute convincing evidence. Following the analysis by *Klimas et al.* [2000] of their one-dimensional current-sheet model, we have studied the transport of electromagnetic (predominantly magnetic) energy in the two-dimensional driven current-sheet model under consideration here. We have found that the portion of the Poynting flux that is due to the presence of resistivity in the MHD plasma exhibits scale-free avalanche distributions over large ranges of the measured avalanche properties. The indices that define these power law distributions are similar to those found by *Uritsky et al.* [2002] in their analysis of the UVI auroral image data. These distributions are the principal result of this paper; they are presented below in section 5. We consider this result an important step toward understanding SOC in a plasma physical context and toward explaining the plasma sheet dynamics of substorm onset.

[11] Before proceeding further, we wish to emphasize that we do not consider the present version of the current-sheet model discussed below to be a realistic model of the plasma sheet but we do feel that this model is relevant enough to suggest the steps that must be taken in that direction. The emphasis in this early stage of this research has been to understand the requirements for the establishment of SOC in as relevant a model of an unstable current sheet as possible. In this paper we present the first results, which indicate strongly that the present model version does, indeed, evolve into SOC under certain conditions. We are unaware of any other current-sheet model that exhibits this property so clearly.

2. Driven 2-D Current-Sheet Model

[12] An important characteristic of this current-sheet model is strong coupling between MHD phenomena at large scales and kinetic phenomena at small scales. This coupling is incorporated through the interaction of three components of the model: (1) a two-dimensional resistive MHD component; (2) a simple equation for the growth and decay of anomalous resistivity; and (3) an idealized representation of a current-driven instability that, through its excitation and quenching, leads to the consequent growth or decay of the anomalous resistivity.

[13] All variables in the model are dimensionless. The relations between dimensionless and dimensional quantities are given in Appendix A. All parameters in the model are listed there also, including the values used to obtain the results discussed below.

2.1. Two-Dimensional Resistive MHD

[14] Taking advantage of the reduction to two dimensions, the MHD component of the model is written for the vector potential A. A polytropic law with $\gamma = 5/3$ is used for the energy equation. The resistivity is written as a diffusion coefficient D. The symbol Δ represents the Laplacian differential operator

$$\frac{\partial \rho}{\partial t} + \nabla \cdot (\rho \mathbf{V}) = 0, \tag{1}$$

$$\frac{\partial \mathbf{V}}{\partial t} + (\mathbf{V} \cdot \nabla)\mathbf{V} = -\frac{1}{4\pi\rho}\nabla A(\Delta A) - \frac{\nabla P}{\rho}, \tag{2}$$

$$\frac{\partial A}{\partial t} + (\mathbf{V} \cdot \nabla)A = D\,\Delta A, \tag{3}$$

and

$$\left(\frac{1}{\gamma - 1}\right)\left[\frac{\partial P}{\partial t} + \mathbf{V} \cdot \nabla P\right] + \left(\frac{\gamma}{\gamma - 1}\right)P(\nabla \cdot \mathbf{V}) = \frac{1}{4\pi}D(\Delta A)^2. \tag{4}$$

2.2. Current-Driven Instability

[15] The current density in the MHD system is given by $J = -\Delta A/\sqrt{8\pi}$. Following *Lu* [1995], an idealized current-driven instability is introduced through

$$Q(|J|) = \begin{cases} D_{\min} & |J| < J_c \\ D_{\max} & |J| > \beta J_c \end{cases}. \tag{5}$$

To explain the notation on the right side of equation (5): at each spatial position, the quantity Q can take one of two values, $D_{\max}$ or $D_{\min} \ll D_{\max}$, depending on the evolution in time of $|J|$ at that position. If $Q = D_{\min}$, it remains at that value until $|J| \geq J_c$, at which time it switches to the value $D_{\max}$. Consequently, Q remains at the value $D_{\max}$ until $|J| \leq$

βJ_c with $\beta < 1$. When $Q = D_{max}$ the current-driven instability is excited, while when $Q = D_{min}$ the instability is quenched. Thus equation (5) represents the saturation or quenching of the current-driven instability, depending on the evolution of the current density at each spatial position and including the common property [*Lu*, 1995] that the threshold for quenching is slightly lower than that for excitation. This is a critical feature of this model that is necessary for generating avalanching that is associated with reconnection; it will be discussed fully below.

2.3. Anomalous Resistivity

[16] The effects of the idealized current-driven instability are seen in the consequent evolution of the anomalous resistivity

$$\frac{\partial D(z,t)}{\partial t} = \frac{Q(|J|) - D}{\tau}. \quad (6)$$

Solutions of equation (6) asymptote exponentially to the value of Q with characteristic timescale τ. If the current-driven instability is quenched, then D either remains at the (small) value D_{min} or, if the instability has previously been excited, it evolves toward D_{min} from larger values. If the current-driven instability is excited then D evolves toward $D_{max} \gg D_{min}$. Thus equation (6) represents the evolution of anomalous resistivity, which is assumed due to the growth or decay of small-scale wave activity following the excitation or quenching of the current-driven instability.

[17] It should be noted that the discussion of D and Q in the preceding paragraphs applies to each spatial position in the plasma, independent of all other positions. In the numerical simulations of this model, the evolution of these quantities is computed at each grid point, independent of all others.

2.4. Discussion

[18] It is generally accepted that the MHD approximation is an appropriate one for describing the large-scale evolution of the magnetotail. The resistive MHD component of the 2-D current-sheet model has been adopted for this purpose. Through the evolution of the MHD plasma, however, small spatial scales with consequent high current density are generated. The inclusion of the idealized current-driven instability in the model is an attempt to partially represent the kinetic effects that are expected and are beyond the limitations of the MHD approximation.

[19] *Lui et al.* [1990, 1991] and *Lui* [1996] have shown that a cross-field current instability can be excited in the plasma sheet when the current sheet is thin; a requirement for excitation is excess current density. Excitation can occur over a broad region of the plasma sheet but its consequences likely depend on distance down the tail. Two possibilities are discussed: (1) direct diversion of a portion of the cross-tail current that can trigger the onset of a substorm in a relatively near-Earth portion of the plasma sheet and (2) the generation of broadband electromagnetic waves in the vicinity and above the ion gyrofrequency that can provide the anomalous resistivity necessary to initiate magnetic reconnection [*Lui et al.*, 1993; *Yoon and Lui*, 1993, 1996]. The instability and resistivity components of the 2-D current-sheet model under discussion here are idealized representations of this second possibility. Following the transition of the switch Q in equation (5) from D_{min} to D_{max} due to an excess current density at some location in the simulated plasma, the exponential growth and saturation of the resistivity D according to equation (6) models the exponential growth and saturation of the wave field associated with the cross-field instability. For the present, all parametric dependencies in the instability, except for the critical current density, have been neglected. An important part of making this model more realistic in the future will be the insertion of these dependencies.

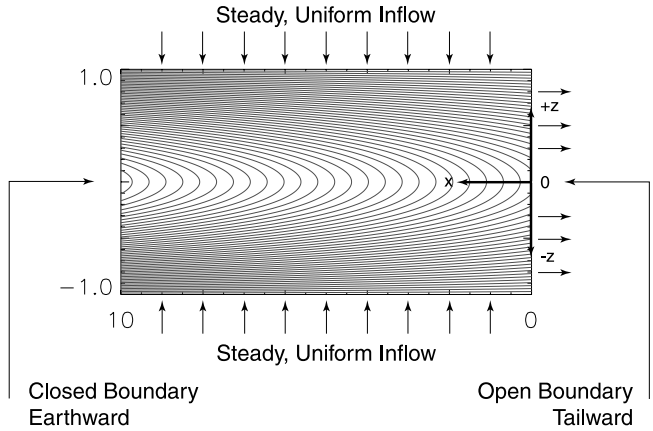

Figure 1. Simulation configuration for the two-dimensional current-sheet model. See color version of this figure in the HTML.

[20] The "hysteresis" ($\beta < 1$) in the Q-switch equation (5) is essential for the model behavior that will be described below. The rationale for this feature and its significance in the model behavior will be discussed below.

3. Simulation Setup and Long-Time Behavior

[21] A system that evolves into SOC is subject to loading and unloading of a conserved quantity. The loading rate is either steady or stochastic with a steady average. The system must be loaded long enough to allow it to establish a time-averaged equilibrium between loading and unloading. The system achieves this equilibrium by self-organizing into a spatial configuration that, though dynamic, remains close to a critical configuration. In this self-organized state, the system exhibits critical point behavior, as discussed above. In order to induce the 2-D current-sheet model into such self-organized critical behavior we have integrated it numerically in the manner illustrated in Figure 1.

3.1. Setup

[22] Initially, inflows are imposed at the upper and lower boundaries of the simulation grid, as indicated in Figure 1 and by equation (C5). The uniform inflow speed and the density at the upper and lower boundaries are then held constant in time for the duration of the simulation. The incoming flows carry magnetic flux in opposing directions at the upper and lower boundaries. The left boundary is closed; plasma can flow along this boundary but not through it. The right boundary is open; plasma can flow along this boundary and through it in the direction out of the

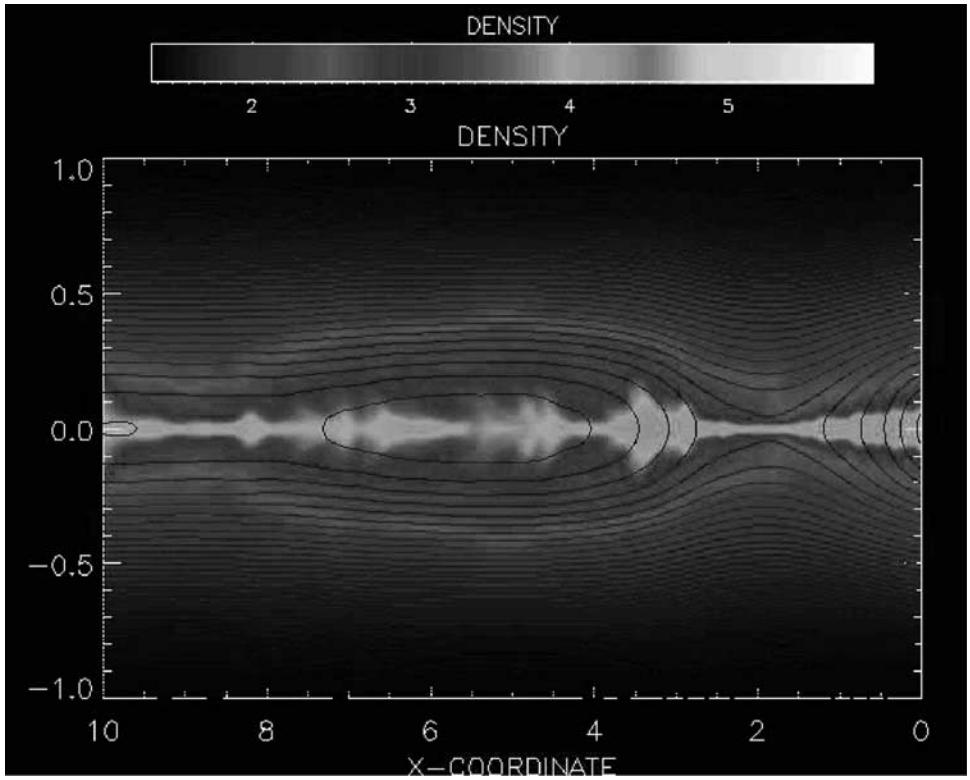

Figure 2. Time-asymptotic plasma sheet-like configuration: magnetic field lines superposed on plasma density. See color version of this figure in the HTML.

simulation region but not into it. The net effect is to load the system with plasma that contains opposing magnetic flux so that the current-sheet strength is increased until the current-driven instability is excited somewhere on the grid. At that point, in a dynamic manner that will be discussed below, the magnetic flux is effectively unloaded from the system by merging and annihilation along the $z = 0$ axis (see Figure 1). Thus the first step toward SOC dynamics, loading and unloading of an otherwise conserved quantity, is achieved. The boundary conditions that are imposed to achieve this behavior are listed in Appendix B.

[23] A force-balanced state (see Appendix C) containing a magnetic field reversal and the supporting current sheet is imposed initially. The equilibrium is imposed to achieve a gentle startup; except for the uniform inflow speed and the density at the upper and lower boundaries that are established in the initial condition, the long-time behavior of the model is independent of the initial state.

3.2. Long-Time Behavior

[24] The long-time state of the model is characterized by a complex current distribution that is, nevertheless, close to the critical current density J_c everywhere in the modeled plasma. Thus the second step toward SOC dynamics, the evolution into criticality, may be achieved. The model evolves toward a state in which the current-driven instability is near its instability threshold throughout.

[25] In the long-time state of the model, the nearly constant current distribution ($J = J_c$) is produced predominantly by a nearly constant gradient $\partial B_x/\partial z$. Solutions are limited to those for which B_x is antisymmetric in z. Thus the field strength at the upper and lower boundaries, as well as the rate at which magnetic flux in driven into the current sheet, is ultimately controlled by the value of the critical current density J_c. If the rate at which magnetic flux is driven into the current sheet is not too large, then the model can take on a plasma sheet-like configuration, as illustrated in Figure 2. The plasma density peaks along $z = 0$ and plasmoid-like shapes emerge in the distributions of density and field lines. As time advances, these plasmoids move out of the system through the open boundary to the right and new ones form to take their place. Figure 2 is a frame from a video animation that is available through an electronic supplement associated with this paper (see DensFL_supp1.mpg)[1]. The formation, propagation, and exiting of these plasmoid-like structures can be viewed in this animation.

[26] If the rate at which magnetic flux is driven into the current sheet is lower than the rate at which it is annihilated, the necessary equality of the time averages of these two rates is achieved through the establishment of a loading-unloading cycle. The annihilation takes place in bursts of activity (unloading interval) interspersed with quiet intervals during which the current-driven instability is not excited anywhere in the simulated plasma, the system reduces to resistive MHD with very low resistivity and the annihilation rate is effectively zero (loading interval since the magnetic flux remains inwardly driven at the

[1] Auxiliary material is available at ftp://ftp.agu.org/apend/ja/2003JA010036.

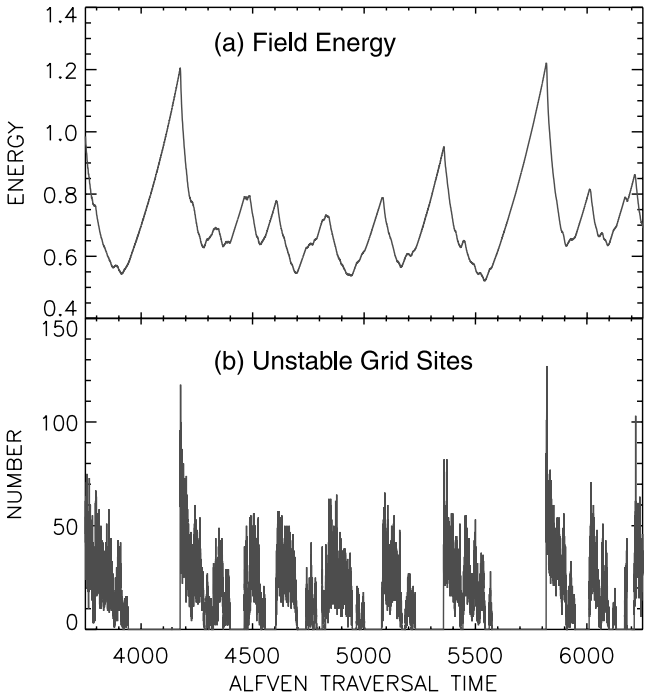

Figure 3. Loading-unloading cycle: (a) total magnetic field energy and (b) number of grid sites at which current-driven instability is excited. See color version of this figure in the HTML.

upper and lower boundaries). Figure 3 shows an example of this cyclical behavior. If the rate at which magnetic flux is driven into the current sheet is increased, the loading intervals shorten until the unloading intervals merge. *Uritsky et al.* [2001b] have demonstrated similar behavior in a one-dimensional reduction of this model and they have shown that strict criticality is lost in that model when the unloading intervals merge.

4. Unloading Onset

[27] Scale-free avalanching is a defining characteristic of numerical SOC models. The Polar UVI image analysis due to *Uritsky et al.* [2002] indicates that in the plasma sheet there may be a scale-free avalanching mechanism related to localized reconnection. The results of Uritsky et al. support the earlier analysis of GEOTAIL plasma sheet data carried out by *Angelopoulos et al.* [1999b] in which in situ evidence for scale-free avalanching related to localized reconnection was developed. In this section, we show that the onset of an unloading interval in the 2-D current-sheet model initiates at a reconnection site and the evolution of the model thereafter has the visual appearance of an avalanche of magnetic field line merging. In the following section, we show that this is, indeed, the onset of a scale-free avalanching process.

4.1. Instability Waves

[28] Figure 4 shows the resistivity distribution D and Figure 5 shows the current density shortly after the onset of an unloading event; these are individual frames from a pair of video animations contained in the electronic supple-

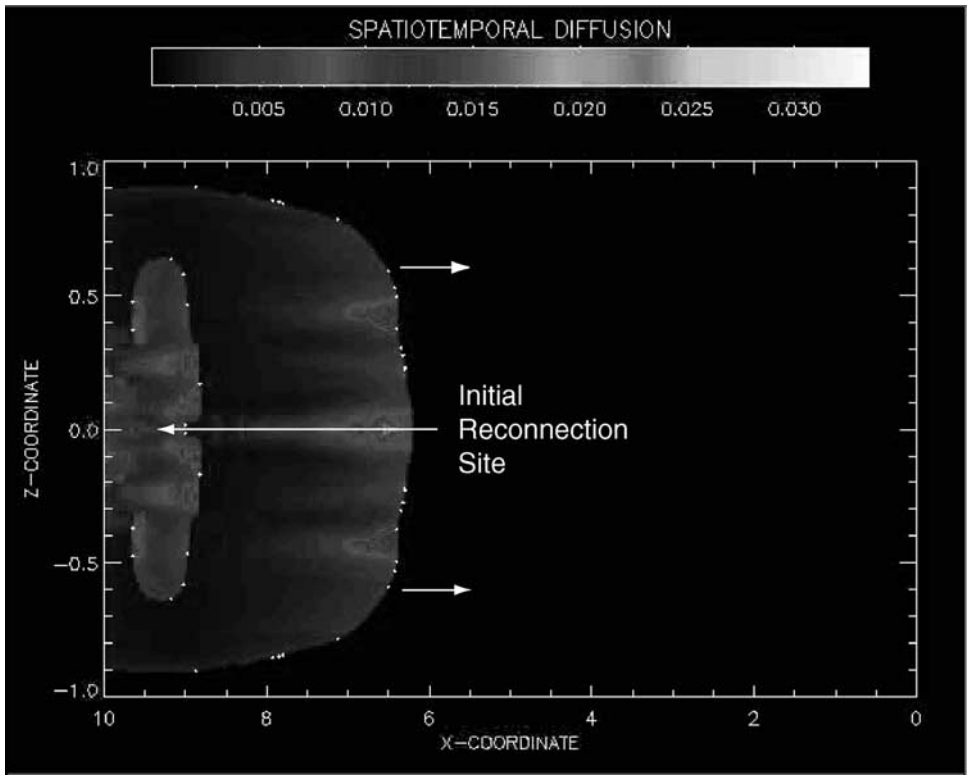

Figure 4. Resistivity distributions shortly after the onset of reconnection at an isolated site. A wave of current-driven instability is spreading away from the reconnection site and a second wave is just emerging; both leave a trail of resistivity in their wakes. See color version of this figure in the HTML.

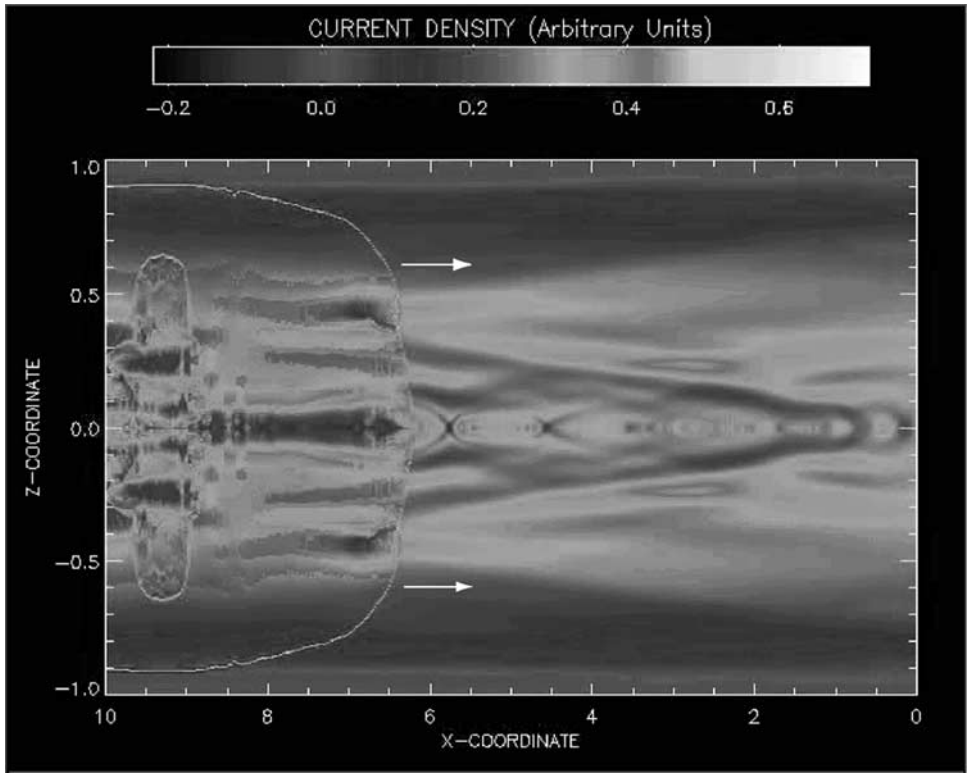

Figure 5. Current density shortly after the onset of reconnection at an isolated site. A wave of intense current is spreading away from the reconnection site and a second wave is just emerging; both are sufficiently strong to excite the current-driven instability. See color version of this figure in the HTML.

ment associated with this paper. (See D_supp3.mpg and J_supp2.mpg for resistivity and current densities, respectively.) The current density had reached the critical current density J_c a short time earlier at the point indicated in the figure, thereby exciting the current-driven instability at that point. A wave of high current density ($\simeq J_c$) can be seen propagating away from the point of initial instability, with a second wave just emerging. The white dots superposed on the resistivity distribution indicate grid positions in the simulation at which the current-driven instability is presently excited. It can be seen that the current density in the propagating wave can be high enough to excite the current-driven instability within the wave. The excitation of this waveform is explained by *Klimas et al.* [2000]. Because the current-driven instability is excited within the wave, the wave is a source of resistivity. The resistivity decays exponentially with rate $1/\tau$ after the wave has passed. The electronic supplement animations should be viewed to see the complex pattern of current and resistivity densities that form as these waves fill the simulation grid.

[29] The point of initial instability in this unloading onset becomes a site of *x* line reconnection that persists thereafter in a dynamic fashion. Still figures are not sufficient for demonstrating this behavior. The third animation in this group (see FL_supp4.mpg), which shows the evolution of the magnetic field lines, illustrates the behavior of the dynamic *x* line. In addition, it can be seen that the generation of resistivity in the waves of instability that propagate away from the reconnection site leads to an expanding region in which the magnetic field becomes unfrozen; an expanding cascade of field line merging results. In effect, the reconnection site broadcasts waves of resistivity that produce what appears to be an expanding avalanche of field line merging.

4.2. Discussion

[30] The behavior described in the preceding section is not typical in MHD simulation codes, even in those in which spatially localized resistivity is turned on at locations where the current has exceeded a predetermined critical value [*Sato and Hayashi*, 1979; *Hoshino*, 1991; *Raeder et al.*, 1996]. The source of this atypical behavior is the hysteresis that has been introduced into the *Q*-switch equation (5) by setting $\beta < 1$. *Lu* [1995] introduced this feature in a continuum SOC model that is the basis for the 2-D current-sheet model under discussion here as well as for the related 1-D model that has been investigated earlier [*Klimas et al.*, 2000; *Uritsky et al.*, 2001a, 2001b]. Lu had two reasons for the introduction of this feature: (1) he showed that it is impossible to achieve avalanching in any continuum (MHD, fluid, etc.) model unless this feature or some equivalent is included and (2) this particular choice mimics the behavior of real plasma instabilities in their nonlinearly saturated states.

4.2.1. Avalanching in Continuum Models

[31] Hysteresis in the local instability is an implicit feature in any discrete SOC model and it must be included in continuum models as well. Without this hysteresis, it is impossible to establish scale-free avalanching. To under-

stand this assertion, reconsider the general properties of systems in SOC that were given above in section 1. Consider a spatially extended system that is subject to loading of a conserved quantity somewhere in the system (at $z = \pm 1$ in the current-sheet model) and unloading at a boundary to the system (the $z = 0$ axis in the current-sheet model). Assume the transport of the conserved quantity is enabled by a local threshold instability that is self-stabilizing (excitation of the instability drives the system back toward local stability) and when excited leads to a rapid, but local, shift of the conserved quantity to neighboring sites in the system. Suppose this process were to leave the originally unstable site at the threshold for the local instability. Then, under continuous loading the system must eventually reach a marginally stable state in which every site is at this instability threshold. In that state, loading of an increment of the conserved quantity anywhere in the system must lead to an avalanche that propagates all the way to the unloading boundary; it would be impossible to develop an internal avalanche. In this case, the dimension of the system is introduced as a characteristic scale for the transport process; the transport process is not scale free. In order for scale-free avalanching to develop, it is necessary that internal avalanches are possible. Internal avalanches are possible only if there are sites within the system that can remain stable even if a neighboring site becomes unstable. Those sites must have been left below the threshold for instability the last time they were involved in the instability process so that they can absorb some amount of the conserved quantity without exceeding the threshold. Hysteresis in the Q-switch equation (5) is one way to obtain this necessary behavior.

[32] It should be noted that the loading-unloading cycle shown in Figure 3 is a direct consequence of the hysteresis in the Q switch. In the absence of hysteresis ($\beta = 1$), a marginally stable quasi steady state is established. If this were the behavior of the plasma sheet in a global magnetospheric model, then it would be impossible to simulate the sequence of substorms [*Farrugia et al.*, 1993; *Freeman and Farrugia*, 1999] that are often observed during extended intervals of relatively steady solar wind conditions containing a strong southward IMF. After a possible initial substorm following the southward turning, the model would necessarily evolve into a quasi steady state with continuous reconnection in the tail. More generally, any loading-unloading behavior in the model would constitute a driven response to the solar wind; the model would not contain an internal loading-unloading response to the solar wind in contrast to the well-known magnetospheric dynamics [*Bargatze et al.*, 1985].

4.2.2. Instability Saturation and Persistence

[33] There may be other ways to generate the necessary behavior discussed in the preceding section, but the Q-switch hysteresis is attractive because consequently the evolution of the anomalous resistivity governed by equation (6) mimics the behavior of real plasma physical instabilities, i.e., the tendency, following the excitation of an instability, for the associated wave field to persist unless the local conditions in the plasma fall below the threshold for the instability. For an elementary example of this behavior, consider a simple one-dimensional electrostatic bump-on-tail instability. A particle beam that leads to a positive slope on the velocity distribution excites the instability. Consequently, resonant modes in the electrostatic field grow and then saturate when the bump on the space-averaged distribution is reduced to a plateau and the positive slope is reduced to zero. At this time, the instability has evolved to marginal stability at its threshold but the wave field that it has generated persists. To quench the wave field, it is necessary, in some way, to reduce the slope on the velocity distribution below the threshold zero value to any negative value, and thereby induce Landau damping. More generally, it is often the case that local instabilities in plasma evolve to a state of marginal stability at the threshold of the instability in the modified state of the plasma, modified through the evolution of the instability. At that time, the wave field that has been generated by the instability persists, pending further developments in the local plasma. One of the many possibilities is a lowering in some way of the state of the plasma to below the locally modified threshold of the instability, thereby quenching the wave field. The evolution of the anomalous resistivity that is generated by equations (5) and (6) mimics this last possibility.

[34] In the specific case of the cross-field current instability [*Lui et al.*, 1990, 1991; *Lui*, 1996], excitation of the instability leads to heating of the local plasma [*Lui et al.*, 1993; *Yoon and Lui*, 1993, 1996] and therefore most likely to a higher threshold for excitation of the instability in the modified plasma state. This threshold increase is not in conflict with the assumption $\beta < 1$ in equation (5). By manually increasing the excitation threshold J_c over the course of an unloading event to simulate its increase with temperature, we have verified that the qualitative evolution of the event is not modified as long as the spread between excitation and quenching thresholds ($\beta < 1$) is maintained. In particular, the instability waves are not quenched even by sudden finite upward jumps in J_c. It is not necessary for the quenching threshold to remain below the original threshold for excitation. If the excitation threshold evolves upward as the instability saturates, then the quenching threshold can evolve upward with it. Although the appropriate temperature dependence of J_c is not included in the 2-D current-sheet model at this time, we are confident that when it is included the behavior discussed in this paper will not be qualitatively modified.

[35] As noted above, all results discussed in this paper were obtained with $\beta = 0.9$. However, we have found that the instability waves propagate even with $\beta = 0.98$; an extremely small spread between excitation and quenching thresholds is sufficient.

5. Avalanche Statistics

[36] To verify the existence of SOC dynamics in the current-sheet model the first step must be a search for behavior that is analogous to the scale-free avalanching of numerical SOC models. A process must be found that leads to the transport of a conserved quantity through the system because of the correlated excitation of a local instability, correlated over spatial and temporal ranges that statistically show no characteristic scales. The results of the preceding section suggest that the conserved quantity may be magnetic flux or energy, which is transported through the model from the upper and lower boundaries to the $z = 0$ axis, where it is

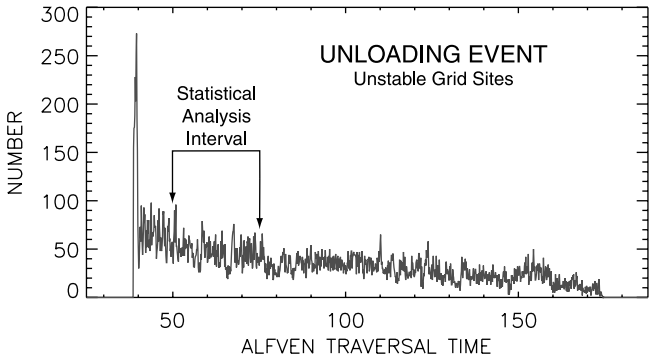

Figure 6. Number of grid sites at which the current-driven instability is excited over the course of a single unloading event. The interval within the event for which avalanche distributions have been constructed is indicated. See color version of this figure in the HTML.

lost to annihilation. The particular transport mode of interest would be that due to the excitation of the current-driven instability, which we have shown above is indeed correlated spatially and temporally through the propagation of the instability waves.

5.1. Diffusive Poynting Flux

[37] Thus (written here in terms of dimensional quantities for clarity) we have studied the transport of the predominantly magnetic, electromagnetic energy density

$$u = \frac{1}{8\pi}\left[E^2 + B^2\right] \tag{7}$$

via the Poynting flux

$$\mathbf{S} = \frac{c}{4\pi}(n\mathbf{J} \times \mathbf{B}) + \frac{1}{4\pi}B^2\mathbf{V}_\perp, \tag{8}$$

in which η is the resistivity. Since it is the first term in this equation that appears to satisfy the requirements discussed above, we have focused our attention on it. We have further restricted our attention to simulations containing a loading-unloading cycle, as discussed above. In such simulations, we have found that during the unloading intervals the diffusive Poynting flux represented by the first term of equation (8) dominates over the convective Poynting flux represented by the second term; both terms are negligibly small during the quiet loading intervals. In the following, we examine the statistical properties of the diffusive transport of electromagnetic energy density in a portion of an unloading event during which the unloading rate is approximately stationary. Figure 6 shows the number of unstable grid sites as a function of time over the course of the unloading event as well as the interval within the unloading event that we have used for this statistical analysis. The rate at which magnetic energy is lost through merging has been found approximately proportional to the number of unstable grid sites.

5.2. Analysis Method

[38] Figure 7 shows the distribution of diffusive Poynting flux magnitude in the simulated plasma at a point in the middle of the statistical analysis interval under consideration. The diffusive flux is dominated strongly by its z component, which is directed toward the $z = 0$ axis from above and below. The diffusive Poynting flux predominantly carries field energy from near the upper and lower boundaries to a region near the $z = 0$ axis where it is converted to

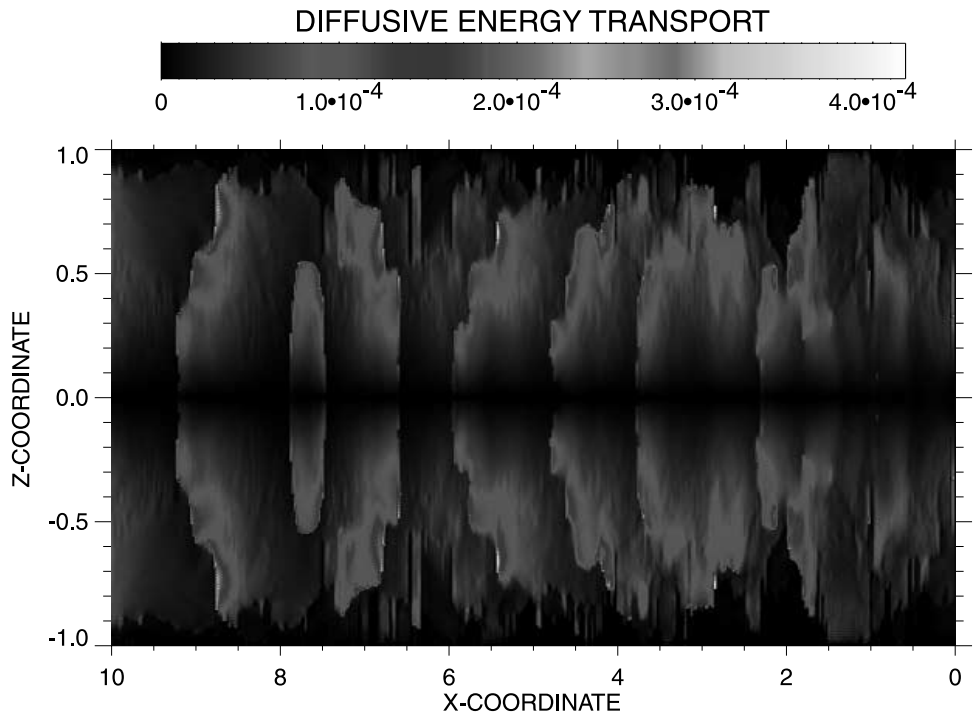

Figure 7. Sample distribution of diffusive Poynting flux magnitude. The x component of this flux is approximately an order of magnitude smaller than the z component, which is directed toward the $z = 0$ axis from above and below. See color version of this figure in the HTML.

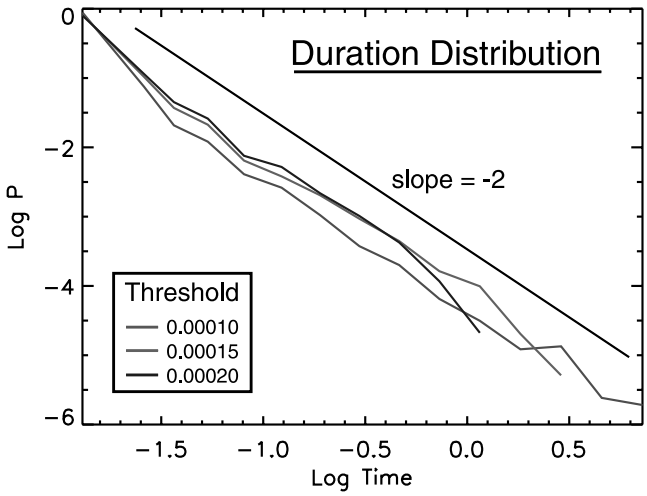

Figure 8. Duration probability distributions of high-transport (H-T) regions in the evolving Poynting flux magnitude over the course of the analysis interval indicated in Figure 6. The H-T regions have been constructed using three threshold values, as indicated. See color version of this figure in the HTML.

plasma thermal and kinetic energy. Only a small portion of the field energy is lost through the open boundary.

[39] We have studied a sequence of 1800 images uniformly spanning the analysis interval indicated in Figure 6. In each of the images, spatial regions were identified, within which the diffusive Poynting flux magnitude was found to exceed a threshold value at contiguous grid sites. These high-transport regions will be called H-T regions in the following. The analysis was carried out three times for three threshold values, 0.001, 0.0015, and 0.002. (See the color bar in (Figure 7) for reference.) Sequential images were examined to find H-T regions that shared common grid sites; those that did were treated as snapshots of the same H-T region as it evolves in time. H-T regions that were not found in two or more consecutive images were ignored. H-T regions that were found to divide into two or more segments were treated, nevertheless, as one region. If H-T regions were found to merge, they were still considered separate regions, with the common merged region treated as the continuation of the region that started earlier. In this way, the H-T regions were examined following the established rules for analyzing the statistical properties of avalanches in running cellular automaton SOC models [*Becker et al.*, 1995]. Further, this analysis follows exactly that of the Polar UVI image data carried out by *Uritsky et al.* [2002].

[40] The final video animation contained in the electronic supplement associated with this paper shows the evolution of the H-T regions for a portion of the analysis interval (See DiffTran_supp5.mpg). The initial frame of this animation shows the same distribution as that shown in Figure 7 except that the threshold value 0.001 has been applied. Only regions of diffusive Poynting flux at or above this threshold appear in the video; these are the evolving H-T regions described in the preceding paragraph.

5.3. Avalanche Distributions

[41] Numerical SOC models exhibit scale-free distributions of certain avalanche measures. To construct these distributions, individual avalanches are followed from beginning to end and properties such as their duration, their total area, some measure of the size (for example, in a sandpile model, the number of grains involved in the avalanche), and others are tabulated. Occurrence distributions are constructed and usually normalized to produce probability distributions for the values of these tabulated properties. For models in SOC, all of these distributions have power law forms containing no characteristic scales.

[42] Analogously, we have followed each of the H-T regions from beginning to end and have recorded their duration, integrated (in time) area, and integrated (space and time) diffusive Poynting flux magnitude. From these data, we have constructed probability distributions for duration, size (integrated area), and energy (integrated Poynting flux magnitude).

[43] Figure 8 shows the probability distributions of the H-T region durations for the three threshold values defined above. Except for the loss of longer duration events for the higher thresholds, the results are relatively insensitive to the threshold value over the range of values shown. A line with slope -2 has been drawn on the figure. The distributions are consistent with scale-free power law distributions with slope close to -2 over slightly less than three decades in duration time.

[44] Figure 9 shows the probability distributions of the H-T region sizes and Figure 10 shows the distributions of energies, both for the three threshold values. Again, the distributions are insensitive to changes of the threshold and, in both instances, are consistent with scale-free power law distributions with slope close to -1.5 over almost five decades in size or energy.

5.4. Discussion

[45] At minimum, the probability distributions shown in Figures 8–10 show that the transport of magnetic field energy into the central annihilation region of the current sheet is carried by an avalanching process that is scale free

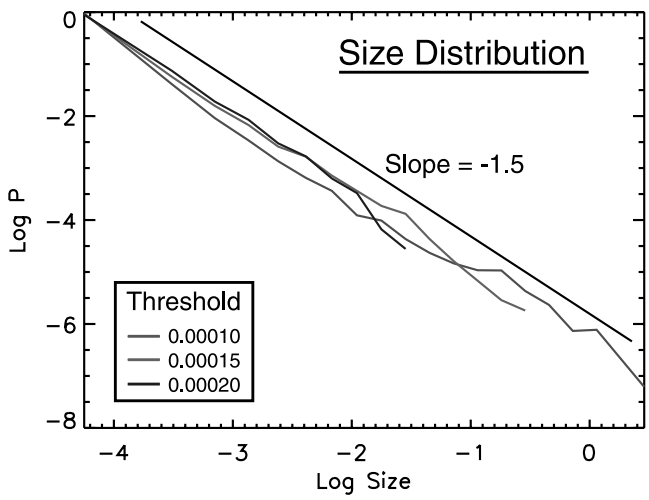

Figure 9. Size probability distribution of high-transport (H-T) regions in the evolving Poynting flux magnitude over the course of the analysis interval indicated in Figure 6. The H-T regions have been constructed using three threshold values, as indicated. See color version of this figure in the HTML.

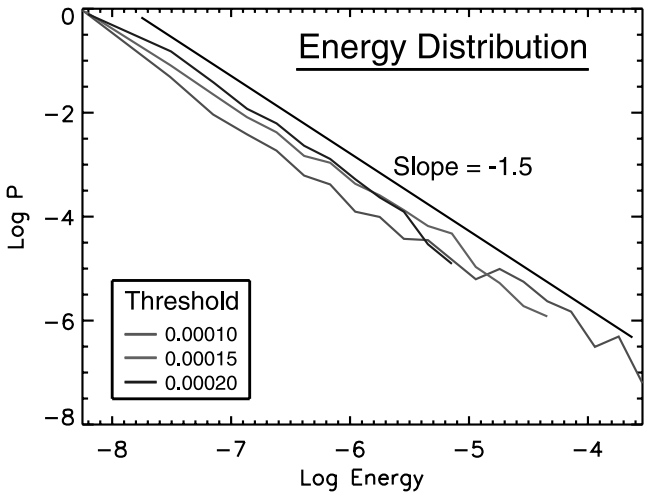

Figure 10. Energy probability distribution of high-transport (H-T) regions in the evolving Poynting flux magnitude over the course of the analysis interval indicated in Figure 6. The H-T regions have been constructed using three threshold values, as indicated. See color version of this figure in the HTML.

over an exceptionally large range of scales. The conclusions that we may draw from this result depend a great deal on the setting in which the avalanching process operates.

[46] The model output that was used to construct the avalanche distributions was taken from a portion of an unloading event that occurred in what we have called the long-time state of the model. As discussed above, this long-time state is characterized by a complex current distribution that is, nevertheless, close to the critical current density J_c everywhere in the modeled plasma. After being disturbed by an unloading event, the model always evolves back toward this state in which the current-driven instability is near its instability threshold throughout; it self-organizes into a state that is consistent with it being in the neighborhood of criticality.

[47] The current-sheet model governs the transport of a conserved quantity, the predominantly magnetic electromagnetic energy. We have shown that the transport of this energy is subject to the excitation of a local instability, the current-driven instability, which through the propagation of the instability waves is correlated spatially and temporally over extended ranges. From the avalanche distributions, we have seen that statistically these correlations are distributed with no characteristic scales over large ranges of scales.

[48] Given (1) the insensitivity of the avalanche distributions to the threshold values used in their construction, (2) the large ranges of scales over which the distributions are scale free, (3) the fact that at least three important quantities, duration, size, and energy, show these scale-free distributions, and (4) the appropriate setting within which the avalanching process operates, we conclude that the scale-free avalanche distributions provide strong evidence that the current-sheet model is in SOC when it is in the long-time state described above.

6. Summary

[49] Through their analysis of Polar UVI image data, *Uritsky et al.* [2002] have produced strong evidence of SOC dynamics in Earth's magnetosphere. The most natural explanation for their results is the existence of a scale-free avalanching process associated with reconnection in the plasma sheet. In fact, there appears to be no other available explanation at present. If this explanation were accepted, however, a fundamental reexamination of the substorm phenomenon in the plasma sheet would become necessary. Substorms would necessarily be viewed as extreme system-wide events in a distribution of events that stretches from global scales down to scales comparable to the upper limit that has been placed on individual localized reconnection events; i.e., $\sim$1 R_E. (Even smaller scales in the plasma sheet are implied by the Uritsky et al. results.) Substorm onset would have to be viewed as an avalanche of localized instabilities that manage, somehow, to evolve in a coordinated fashion. Such a major paradigm shift should be approached with some caution. While the Uritsky et al. evidence is strong, the UVI image results provide only a remote measure of the plasma sheet dynamics. In situ plasma sheet observations must be the next step.

[50] It would be necessary to study the multispatiotemporal-scale behavior of the plasma sheet to confirm its SOC dynamics. Generally, with some dependence on phase in the substorm cycle, long-ranged correlated behavior should be expected. The multispacecraft Cluster and MMS missions would make such a study possible. However, SOC dynamics in a plasma physical setting is largely unexplored and consequently it is impossible at this time to suggest specific goals for such a study.

[51] Therefore we have embarked on a study of SOC in models of the magnetic field reversal and driven reconnection of the plasma sheet. We have incorporated strongly coupled MHD and kinetic components in the models so that multiscale dynamics over the extremely broad range shown by *Uritsky et al.* [2002] may result. For the kinetic component, anomalous resistivity due to a current-driven instability in the plasma is incorporated in a manner suggested by *Lu* [1995]. We have shown earlier that a one-dimensional model of this kind does evolve into SOC under steady driving. Here we have discussed a two-dimensional model and have presented the first evidence that it too evolves into SOC when driven continuously.

[52] *Lu* [1995] has shown that it is impossible to produce scale-free avalanching in any driven continuum model unless the local threshold instability that is involved in the transport of the conserved quantity through the system is hysteretic. The threshold for quenching the instability must be at least slightly below its threshold for excitation. A macroscopic consequence of this property is a loading-unloading cycle. Simply put, cumulative activity at the kinetic level persists long enough to drive the macrosystem below its threshold for unloading so that subsequently it must be loaded for some time before it can reach that threshold again. Lu has shown, and we have confirmed, that should the local instability have no hysteresis, then the macrosystem must evolve to a steady marginally stable state under continuous loading; a loading-unloading cycle is then impossible. As an example, we have discussed a single kinetic instability, the bump-on-tail instability, and have shown that it does exhibit this hysteretic property. We have further suggested, following Lu, that this is a common property of other kinetic instabilities. We will report in the

future on a simulation study of the relevant cross-field current instability [*Lui*, 2002] in which we will verify this property of the instability.

[53] We have shown that an interesting consequence of hysteresis in the current-driven instability is the possible propagation of current sheets whose strengths are sufficient to excite the instability. We have found that unloading events in the model evolution all start at the onset of local reconnection at a site that then becomes a source for many of these propagating current sheets. As these current sheets propagate away from the reconnection site, since they are intense enough to excite the current-driven instability, they leave trails of anomalous resistivity in their wakes. Thus the original isolated reconnection site becomes the origin of an expanding region of field line merging as this resistivity spreads. We suggest this behavior as a possible mechanism for localized reconnection-associated avalanching in the plasma sheet. The expanding current-sheet waves can provide the necessary long-ranged correlated behavior in the plasma and, as we have shown, the expanding cascade of field line merging does lead to scale-free avalanching.

[54] We have examined the transport of (predominantly) magnetic energy from the exterior boundaries of the simulation grid, where it is driven into the simulated plasma, to the interior neutral sheet where it is annihilated. There are two contributions to this transport, the motion of the frozen-in field lines with the plasma and the diffusive transport enabled by the excitation of the current-driven instability. The second of these contributions is dominant during the modeled unloading events and it is most analogous to the transport mechanisms found in discrete SOC models. Thus we have focused our attention on the diffusive transport of magnetic energy through the plasma.

[55] Using methods that have been developed for analyses of running-sandpile models [*Becker et al.*, 1995], we have studied some statistical properties of the magnetic energy diffusive transport during an unloading event. Three threshold values were set and for each value contiguous spatial regions where the diffusive Poynting flux rose above the threshold were identified and followed in time. The duration of each of these regions, their integrated area, and the magnetic energy that they transported were tabulated. Probability distributions for each of these properties were constructed for each of the threshold values. We have shown that each of these avalanche distributions is of a scale-free power law form and that the distributions are stable under the changes in threshold value that we have applied. The distributions are remarkably similar to the distributions that *Uritsky et al.* [2002] found for duration, integrated size, and integrated energy of auroral emission regions in their analysis of Polar UVI image data. We have no explanation for this interesting result at present but, of course, we will investigate it in the future. Given (1) the insensitivity of the avalanche distributions to the threshold values used in their construction, (2) the large ranges of scales over which the distributions are scale free, (3) the fact that at least three important quantities, duration, size, and energy, show these scale-free distributions, and (4) the appropriate setting within which the avalanching process operates, we conclude that the scale-free avalanche distributions provide strong evidence that the 2-D current-sheet model can evolve into SOC when driven steadily.

[56] On the basis of this initial success, we are proceeding ahead with an analysis of the susceptibility [*Vespignani and Zapperi*, 1998] of the 2-D current sheet model to provide conclusive evidence that it can evolve into SOC. Concurrently, we will generalize the model to approximate the plasma sheet more accurately. The principal area of concern is the parametric dependence of the cross-field current instability threshold, which has not been included properly at present. When a more realistic representation of the effects of this instability is included, it will become possible to restrict the parameters of the model to values that represent the plasma sheet better. A further generalization of the model to three dimensions is anticipated. As the model is improved, we expect that it will suggest multi-spacecraft in situ studies of the plasma sheet to test our assertion that the *Uritsky et al.* [2002] results imply SOC dynamics in the plasma sheet.

Appendix A

A1. Dimensionless Variables

[57] The current-sheet model is simulated on the two-dimensional (x, z) grid, as indicated in Figure 1. Lengths are measured in units of the half-thickness L_z of the current sheet in the z direction. In the following, dimensionless variables are indicated by starred symbols

$$z^* = \frac{z}{L_z}, \tag{A1}$$

$$x^* = \frac{x}{L_z} = \varepsilon^{-1}\frac{x}{L_x}, \qquad (\varepsilon = L_z/L_x), \tag{A2}$$

and

$$B_0 \equiv B_x(x = L_x, kz = 1), \tag{A3}$$

in which k is a parameter that is introduced to allow for flexibility in the initial state of the simulation (see equations (C1) and (C2)).

$$\mathbf{B}^* = \frac{\mathbf{B}}{B_0} = \frac{1}{\sqrt{8\pi}}\nabla^* \times \mathbf{A}^*, \tag{A4}$$

$$A^* = \frac{\sqrt{8\pi}}{L_z B_0}A, \tag{A5}$$

$$\rho^* = \frac{\rho}{\rho_0}, \qquad \rho_0 = \rho(kz = 1), \tag{A6}$$

$$\mathbf{V}^* = \frac{\mathbf{V}}{V_A}, \qquad V_A = \frac{B_0}{\sqrt{8\pi\rho_0}}, \tag{A7}$$

$$t^* = \left(\frac{V_A}{L_z}\right)t, \tag{A8}$$

$$D^* = \frac{D}{L_z V_A}, \qquad D = \frac{c^2}{4\pi}\eta, \tag{A9}$$

and

$$P^* = \frac{P}{\left(B_0^2/8\pi\right)}. \tag{A10}$$

A2. Parameters

[58] The parameters that have been used to obtain the solutions of the current-sheet model discussed in this paper are given by $\varepsilon = L_z/L_x = 0.1$, $\gamma = 5/3$, $k = 0.3$, $x_0 = 50.0$ (see equations (C1) and (C2)), $V_b = 0.001$ (see equation (C5)), $J_c = 0.45$, $P_0 = 0.1$, $\tau = 1.0$, $\beta = 0.9$, $D_{\min} = 10^{-6}$, $D_{\max} = 4.0$, grid spacing $\Delta_x = 0.025$, $\Delta_z = 0.005$, and integration time step $\Delta_t = 0.00025$.

Appendix B: Boundary Conditions

$z = 0$

$$\begin{gathered}
\partial A(x,0)/\partial z = 0 \\
\partial V_x(x,0)/\partial z = 0 \\
V_z(x,-\Delta_z) = -V_z(x,\Delta_z) \\
\partial \rho(x,0)/\partial z = 0 \\
\partial P(x,0)/\partial z = 0
\end{gathered} \tag{B1}$$

$z = 1$

$$\begin{gathered}
\partial^2 A(x,1)/\partial z^2 = 0 \\
\partial V_x(x,1)/\partial z = 0 \\
V_z(x,\text{bndry}) = \text{initial condition} \\
\rho(\text{x},\text{bndry}) = \text{initial condition} \\
\partial P(x,1)/\partial z = 0
\end{gathered} \tag{B2}$$

$x = 0$

$$\begin{gathered}
\partial^2 A(0,z)/\partial x^2 = 0 \\
\partial V_x(0,z)/\partial x = 0 \\
\partial V_z(0,z)/\partial x = 0 \\
\partial^2 \rho(0,z)/\partial x^2 = 0 \\
\partial^2 P(0,z)/\partial x^2 = 0
\end{gathered} \tag{B3}$$

but $V_x\,(0, z) \leq 0$.

$x = 1/\varepsilon$

$$\begin{gathered}
\partial A(1/\varepsilon,z)/\partial x = 0 \\
V_x(1/\varepsilon + \Delta_x, z) = -V_x(1/\varepsilon - \Delta_x, z) \\
\partial V_z(1/\varepsilon,z)/\partial x = 0 \\
\partial \rho(1/\varepsilon,z)/\partial x = 0 \\
\partial P(1/\varepsilon,z)/\partial x = 0.
\end{gathered} \tag{B4}$$

In addition, weak diffusive smoothing has been applied in a thin layer at the open boundary in order to prevent excitation of instability waves due to slight irregularities at the boundary.

Appendix C: Initial Conditions

$$A(x,z,t=0) = \sqrt{8\pi}\left(\frac{2}{k\pi}\right)\sin\left(\frac{\pi}{2}\right)\left[\frac{\varepsilon(x+x_0)}{1+\varepsilon x_0}\right]\cos\left(\frac{k\pi z}{2}\right) \tag{C1}$$

$$\begin{aligned}
P(x,z,t=0) = P_0 + &\left[1+\left(\frac{1}{k}\right)^2\left(\frac{\varepsilon}{1+\varepsilon x_0}\right)^2\right] \\
&\cdot \sin^2\left(\frac{\pi}{2}\right)\left[\frac{\varepsilon(x+x_0)}{1+\varepsilon x_0}\right]\cos^2\left(\frac{k\pi z}{2}\right)
\end{aligned} \tag{C2}$$

$$\rho(x,z,t=0) = \left(\frac{P(x,z,t=0)}{P_0}\right)^{1/\gamma} \tag{C3}$$

$$V_x(x,z,t=0) = 0 \tag{C4}$$

$$V_z(x,z,t=0) = -V_b\left[\frac{1-\cos(\pi z/2)}{\sin(\pi z/2)}\right]. \tag{C5}$$

[59] **Acknowledgments.** This work was supported by NASA RTOP grant 344-14-00-02. We thank T. Chang, A. T. Y. Lui, D. H. Fairfield, G. Consolini, S. C. Chapman, N. W. Watkins, G. Parks, and J. Birn for valuable discussions.

[60] Lou-Chuang Lee thanks Tom Chang for the assistance in evaluating this paper.

References

Angelopoulos, V., W. Baumjohann, C. F. Kennel, F. V. Coroniti, M. G. Kivelson, R. Pellat, R. J. Walker, H. Luhr, and G. Paschmann (1992), Bursty bulk flows in the inner central plasma sheet, *J. Geophys. Res.*, *97*(A4), 4027–4039.

Angelopoulos, V., C. F. Kennel, F. V. Coroniti, R. Pellat, M. G. Kivelson, R. J. Walker, C. T. Russell, W. Baumjohann, W. C. Feldman, and J. T. Gosling (1994), Statistical characteristics of bursty bulk flow events, *J. Geophys. Res.*, *99*(A11), 21,257–21,280.

Angelopoulos, V., et al. (1996), Multipoint analysis of a bursty bulk flow event on April 11, 1985, *J. Geophys. Res.*, *101*(A3), 4967–4989.

Angelopoulos, V., F. S. Mozer, T. Mukai, K. Tsuruda, S. Kokubun, and T. J. Hughes (1999a), On the relationship between bursty flows, current disruption and substorms, *Geophys. Res. Lett.*, *26*(18), 2841–2844.

Angelopoulos, V., T. Mukai, and S. Kokubun (1999b), Evidence for intermittency in Earth's plasma sheet and implications for self-organized criticality, *Phys. Plasmas*, *6*(11), 4161–4168.

Bak, P. (1997), *How Nature Works: The Science of Self-Organized Criticality*, 212 pp., Oxford Univ. Press, New York.

Bak, P., C. Tang, and K. Wiesenfeld (1987), Self-organized criticality: An explanation of 1/*f* noise, *Phys. Rev. Lett.*, *59*(4), 381–384.

Bak, P., C. Tang, and K. Wiesenfeld (1988), Self-organized criticality, *Phys. Rev. A Gen. Phys.*, *38*(1), 364–374.

Baker, D. N., T. I. Pulkkinen, J. Buchner, and A. J. Klimas (1999), Substorms: A global instability of the magnetosphere-ionosphere system, *J. Geophys. Res.*, *104*(A7), 14,601–14,611.

Bargatze, L. F., D. N. Baker, R. L. McPherron, and E. W. Hones (1985), Magnetospheric impulse response for many levels of geomagnetic activity, *J. Geophys. Res.*, *90*(A7), 6387–6394.

Baumjohann, W., G. Paschmann, and H. Luhr (1990), Characteristics of high-speed ion flows in the plasma sheet, *J. Geophys. Res.*, *95*(A4), 3801–3809.

Becker, T., H. Devries, and B. Eckhardt (1995), Dynamics of a stochastically driven running sandpile, *J. Nonlinear Sci.*, *5*(2), 167–188.

Blanchard, G. T., L. R. Lyons, and J. Spann (2000), Predictions of substorms following northward turnings of the interplanetary magnetic field, *J. Geophys. Res.*, *105*(A1), 375–384.

Borovsky, J. E., R. C. Elphic, H. O. Funsten, and M. F. Thomsen (1997), The Earth's plasma sheet as a laboratory for flow turbulence in high-beta MHD, *J. Plasma Phys.*, *57*, 1–34.

Chang, T. (1992a), Low-dimensional behavior and symmetry breaking of stochastic systems near criticality—Can these effects be observed in space and in the laboratory, *IEEE Trans. Plasma Sci.*, *20*(6), 691–694.

Chang, T. (1992b), Path-integrals, differential renormalization-group, and stochastic-systems near criticality, *Int. J. Eng. Sci.*, *30*(10), 1401–1405.

Chang, T. (1998), Sporadic localized reconnections and intermittent turbulence in the magnetotail, in *Geospace Mass and Energy Flow*, edited by J. L. Horwitz, D. L. Gallagher, and W. K. Peterson, 193 pp., AGU, Washington, D. C.

Chang, T. (1999), Self-organized criticality, multi-fractal spectra, sporadic localized reconnections and intermittent turbulence in the magnetotail, *Phys. Plasmas*, *6*(11), 4137–4145.

Chang, T., and C. Wu (2002), "Complexity" and anomalous transport in space plasmas, *Phys. Plasmas*, *9*(9), 3679–3684.

Chang, T., C. C. Wu, and V. Angelopoulos (2002), Preferential acceleration of coherent magnetic structures and bursty bulk flows in Earth's magnetotail, *Phys. Scripta T*, *98*, 48–51.

Chapman, S. C. (2000), Inverse cascade avalanche model with limit cycle exhibiting period doubling, intermittency, and self-similarity, *Phys. Rev. E*, *62*(2), 1905–1911.

Chapman, S. C., N. W. Watkins, R. O. Dendy, P. Helander, and G. Rowlands (1998), A simple avalanche model as an analogue for magnetospheric activity, *Geophys. Res. Lett.*, *25*(13), 2397–2400.

Chapman, S. C., R. O. Dendy, and G. Rowlands (1999), A sandpile model with dual scaling regimes for laboratory, space and astrophysical plasmas, *Phys. Plasmas*, *6*(11), 4169–4177.

Farrugia, C. J., M. P. Freeman, L. F. Burlaga, R. P. Lepping, and K. Takahashi (1993), The Earth's magnetosphere under continued forcing: Substorm activity during the passage of an interplanetary magnetic cloud, *J. Geophys. Res.*, *98*(A5), 7657–7671.

Freeman, M. P., and C. J. Farrugia (1999), Solar wind input between substorm onsets during and after the October 18–20, 1995, magnetic cloud, *J. Geophys. Res.*, *104*(A10), 22,729–22,744.

Hoshino, M. (1991), Forced magnetic reconnection in a plasma sheet with localized resistivity profile excited by lower hybrid drift type instability, *J. Geophys. Res.*, *96*(A7), 11,555–11,567.

Ieda, A., D. H. Fairfield, T. Mukai, Y. Saito, S. Kokubun, K. Liou, C.-I. Meng, G. K. Parks, and M. J. Brittnacher (2001), Plasmoid ejection and auroral brightenings, *J. Geophys. Res.*, *106*(A3), 3845–3857.

Jensen, H. J. (1998), *Self-Organized Criticality: Emergent Complex Behaviour in Physical and Biological Systems*, Cambridge Univ. Press, New York.

Klimas, A. J., D. Vassiliadis, and D. N. Baker (1996), The nonlinear dynamics of the magnetosphere: Where are we now?, in *Multiscale Phenomena in Space Plasmas*, edited by T. Chang, 299 pp., Scientific, Gainesville, Fla.

Klimas, A. J., J. A. Valdivia, D. Vassiliadis, D. N. Baker, M. Hesse, and J. Takalo (2000), Self-organized criticality in the substorm phenomenon and its relation to localized reconnection in the magnetospheric plasma sheet, *J. Geophys. Res.*, *105*(A8), 18,765–18,780.

Lu, E. T. (1995), Avalanches in continuum driven dissipative systems, *Phys. Rev. Lett.*, *74*(13), 2511–2514.

Lui, A. T. Y. (1996), Current disruption in the Earth's magnetosphere: Observations and models, *J. Geophys. Res.*, *101*(A6), 13,067–13,088.

Lui, A. T. Y. (2002), Particle simulation of the cross-field current instability in a thin current sheet, in *Sixth International Conference on Substorms*, edited by R. M. Winglee, pp. 25–32, Univ. of Wash., Seattle.

Lui, A. T. Y., A. Mankofsky, C. L. Chang, K. Papadopoulos, and C. S. Wu (1990), A current disruption mechanism in the neutral sheet—A possible trigger for substorm expansions, *Geophys. Res. Lett.*, *17*(6), 745–748.

Lui, A. T. Y., C. L. Chang, A. Mankofsky, H. K. Wong, and D. Winske (1991), A cross-field current instability for substorm expansions, *J. Geophys. Res.*, *96*(A7), 11,389–11,401.

Lui, A. T. Y., P. H. Yoon, and C. L. Chang (1993), Quasi-linear analysis of ion weibel instability in the Earth's neutral sheet, *J. Geophys. Res.*, *98*(A1), 153–163.

Lui, A. T. Y., S. C. Chapman, K. Liou, P. T. Newell, C. I. Meng, M. Brittnacher, and G. D. Parks (2000), Is the dynamic magnetosphere an avalanching system?, *Geophys. Res. Lett.*, *27*(7), 911–914.

Lyons, L. R. (2000), Geomagnetic disturbances: Characteristics of, distinction between types, and relations to interplanetary conditions, *J. Atmos. Sol. Terr. Phys.*, *62*(12), 1087–1114.

Lyons, L. R., G. T. Blanchard, J. C. Samson, R. P. Lepping, T. Yamamoto, and T. Moretto (1997), Coordinated observations demonstrating external substorm triggering, *J. Geophys. Res.*, *102*(A12), 27,039–27,051.

Nakamura, R., W. Baumjohann, M. Brittnacher, V. A. Sergeev, M. Kubyshkina, T. Mukai, and K. Liou (2001a), Flow bursts and auroral activations: Onset timing and foot point location, *J. Geophys. Res.*, *106*(A6), 10,777–10,789.

Nakamura, R., W. Baumjohann, R. Schodel, M. Brittnacher, V. A. Sergeev, M. Kubyshkina, T. Mukai, and K. Liou (2001b), Earthward flow bursts, auroral streamers, and small expansions, *J. Geophys. Res.*, *106*(A6), 10,791–10,802.

Raeder, J., J. Berchem, and M. Ashour-Abdalla (1996), The importance of small scale processes in global MHD simulations: Some numerical experiments, in *The Physics of Space Plasmas*, edited by T. Chang and J. R. Jasperse, 403 pp., MIT Cent. for Theor. Geo/Cosmo Plasma Phys., Cambridge, Mass.

Russel, C. T. (2000), How northward turnings of the IMF can lead to substorm expansion onsets, *Geophys. Res. Lett.*, *27*(20), 3257–3259.

Sato, T., and T. Hayashi (1979), Externally driven magnetic reconnection and a powerful magnetic energy converter, *Phys. Fluids*, *22*(6), 1189–1202.

Sharma, A. S. (1995), Assessing the magnetospheres nonlinear behavior—Its dimension is low, its predictability, *Rev. Geophys.*, *33*, 645–650.

Uritsky, V. M., A. J. Klimas, J. A. Valdivia, D. Vassiliadis, and D. N. Baker (2001a), Stable critical behavior and fast field annihilation in a magnetic field reversal model, *J. Atmos. Sol. Terr. Phys.*, *63*(13), 1425–1433.

Uritsky, V. M., A. J. Klimas, and D. Vassiliadis (2001b), Multiscale dynamics and robust critical scaling in a continuum current sheet model, *Phys. Rev. E*, *65*(4).

Uritsky, V. M., A. J. Klimas, D. Vassiliadis, D. Chua, and G. D. Parks (2002), Scale-free statistics of spatiotemporal auroral emissions as depicted by Polar UVI images: The dynamic magnetosphere is an avalanching system, *J. Geophys. Res.*, *107*(A12), 1426, doi:10.1029/2001JA000281.

Vassiliadis, D., A. J. Klimas, D. N. Baker, and D. A. Roberts (1995), A description of the solar-wind magnetosphere coupling based on nonlinear filters, *J. Geophys. Res.*, *100*(A3), 3495–3512.

Vespignani, A., and S. Zapperi (1998), How self-organized criticality works: A unified mean-field picture, *Phys. Rev. E*, *57*(6), 6345–6362.

Vörös, Z., et al. (2003), Multi-scale magnetic field intermittence in the plasma sheet, *Ann. Geophys.*, *21*(9), 1955–1964.

Watkins, N. W., S. C. Chapman, R. O. Dendy, and G. Rowlands (1999), Robustness of collective behaviour in strongly driven avalanche models: Magnetospheric implications, *Geophys. Res. Lett.*, *26*(16), 2617–2620.

Yoon, P. H., and A. T. Y. Lui (1993), Nonlinear-analysis of generalized cross-field current instability, *Phys. Fluids A*, *5*(3), 836–853.

Yoon, P. H., and A. T. Y. Lui (1996), Nonlocal ion Weibel instability in the geomagnetic tail, *J. Geophys. Res.*, *101*(A3), 4899–4906.

Zesta, E., L. R. Lyons, and E. Donovan (2000), The auroral signature of earthward flow bursts observed in the magnetotail, *Geophys. Res. Lett.*, *27*(20), 3241–3244.

D. N. Baker, Laboratory for Atmospheric and Space Physics, University of Colorado at Boulder, Boulder, CO 80309, USA. (baker@lynx.colorado.edu)

A. J. Klimas, Laboratory for Extraterrestrial Physics, NASA Goddard Space Flight Center, 8800 Greenbelt Road, Mail Code 692, Bldg. 21, Room 265A, Greenbelt, MD 20771, USA. (alex.klimas@gsfc.nasa.gov)

V. M. Uritsky, Institute of Physics and Physics Department, St. Petersburg State University, St. Petersburg 198504, Russia. (uritsky@geo.phys.spbu.ru)

D. Vassiliadis, Universities Space Research Association, NASA Goddard Space Flight Center, Greenbelt, MD 20771, USA. (vassi@electra.gsfc.nasa.gov)